Cyclewise Operation of Printed MoS$_2$ Transistor Biosensors for Rapid Biomolecule Quantification at Femtomolar Levels

Byunghoon Ryu,[†,§] Hongsuk Nam,[†,§] Bo-Ram Oh,[†] Yujing Song,[†] Pengyu Chen,[†] Younggeun Park,[†] Wenjie Wan,[‡] Katsuo Kurabayashi,[†] and Xiaogan Liang*,[†]

[†]Mechanical Engineering, University of Michigan, Ann Arbor, Michigan 48109, United States
[‡]University of Michigan-Shanghai Jiao Tong University Joint Institute and Department of Physics and Astronomy, Shanghai Jiao Tong University, Shanghai 200240, China

S Supporting Information

ABSTRACT: Field-effect transistors made from MoS$_2$ and other emerging layered semiconductors have been demonstrated to be able to serve as ultrasensitive biosensors. However, such nanoelectronic sensors still suffer seriously from a series of challenges associated with the poor compatibility between electronic structures and liquid analytes. These challenges hinder the practical biosensing applications that demand rapid, low-noise, highly specific biomolecule quantification at femtomolar levels. To address such challenges, we study a cyclewise process for operating MoS$_2$ transistor biosensors, in which a series of reagent fluids are delivered to the sensor in a time-sequenced manner and

periodically set the sensor into four assay-cycle stages, including incubation, flushing, drying, and electrical measurement. Running multiple cycles of such an assay can acquire a time-dependent sensor response signal quantifying the reaction kinetics of analyte-receptor binding. This cyclewise detection approach can avoid the liquid-solution-induced electrochemical damage, screening, and nonspecific adsorption to the sensor and therefore improves the transistor sensor's durability, sensitivity, specificity, and signal-to-noise ratio. These advantages in combination with the inherent high sensitivity of MoS$_2$ biosensors allow for rapid biomolecule quantification at femtomolar levels. We have demonstrated the cyclewise quantification of Interleukin-1β in pure and complex solutions (e.g., serum and saliva) with a detection limit of ~1 fM and a total detection time ~23 min. This work leverages the superior properties of layered semiconductors for biosensing applications and advances the techniques toward realizing fast real-time immunoassay for low-abundance biomolecule detection.

KEYWORDS: biosensor, transistor, transition metal dichalcogenide, nanoelectronics, semiconductor, streptavidin
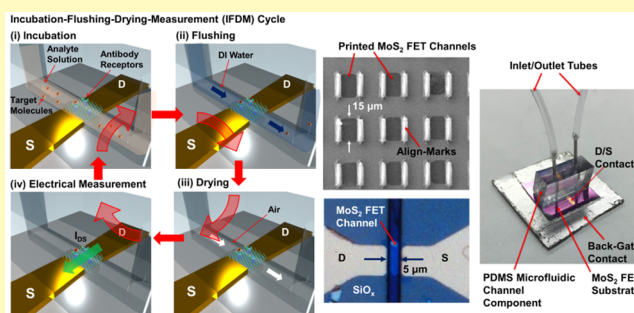
Field-effect transistor (FET) biosensors made from emerging layered transition metal dichalcogenides (TMDCs), such as MoS$_2$ and WSe$_2$, have exhibited attractive characteristics, such as high biodetection sensitivity, low limit-of-detection (LOD), and good compatibility with planar nanofabrication processes, potentially enabling multiplexing sensor arrays. Specifically, Wang et al. and Sarkar et al. demonstrated MoS$_2$ FET biosensors with femtomolar (fM)-level detection limits.[1,2] Nam et al. established the device physics for calibrating the sensor response signals measured from MoS$_2$ FET sensors with insulating layers and preliminarily demonstrated the fabrication of MoS$_2$ FET arrays.[3,4] Lee et al. demonstrated that antibody receptors can be directly grafted on MoS$_2$ FET channels without using insulating layers, which is due to the hydrophobicity of the MoS$_2$ surface.[5] Such an insulating-layer-free sensor structure can significantly lower the fabrication complexity and cost of MoS$_2$ biosensors. Nam et al. further found that insulating-layer-free MoS$_2$ sensors exhibit a higher sensitivity than insulating-layer-coated ones.[6] This was attributed to the fact that two mechanisms, target-molecule-

induced electrostatic doping and target-molecule-induced surface scattering of carriers, synergistically affect the response signal of an insulating-layer-free sensor, but only target-molecule-induced electrostatic doping contributes to the response signal of an insulating-layer-coated sensor.[6,7] Nam et al. also demonstrated that WSe$_2$ FET sensors exhibit a higher sensitivity than MoS$_2$ FET sensors, which is attributed to the ambipolar transfer characteristics of WSe$_2$ FETs.[7]

In spite of the progress mentioned above, MoS$_2$ and other TMDC-based FET biosensors still suffer seriously from a series of challenges that hinder their practical biosensing applications. Especially, a FET sensor needs to be continuously exposed to a liquid reagent environment for quantifying the time-dependent reaction kinetics of analyte-receptor binding. Such a time-dependent detection capability is a key to realize rapid
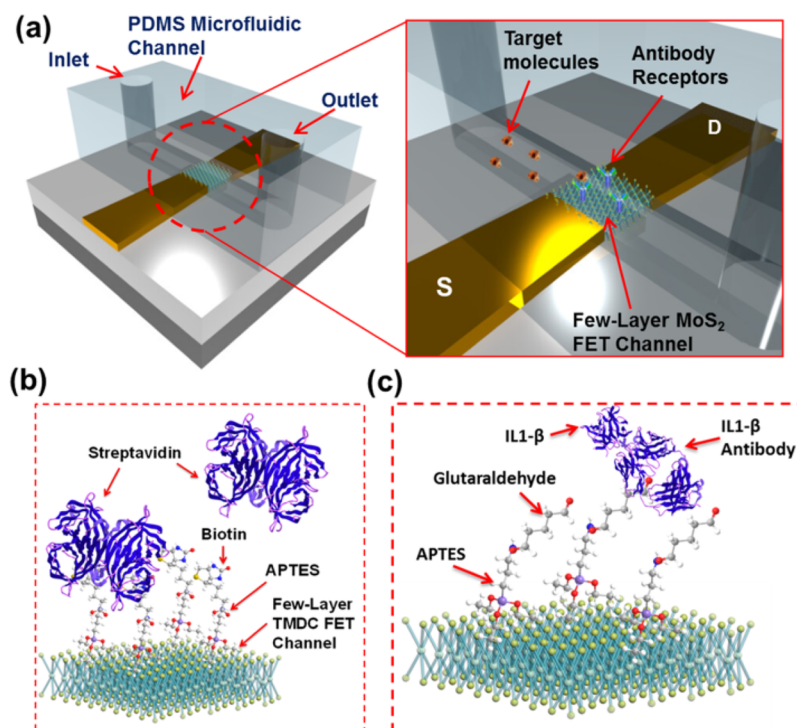
Figure 1. Experimental method: (a) illustration of a MoS$_2$-based FET sensor, which is integrated with a PDMS microfluidic structure and (b, c) illustrations of the TMDC channels functionalized with biotin and IL-1β receptors, respectively.

biomolecule quantification based on sensor response readings at the nonequilibrium states of binding reactions, which could result in very short lapsed times and enable fast real-time immunoassay for quantifying extreme low-abundance biomolecules (e.g., fM-level biomarkers).[8] However, the electrical signal acquisition process is not generally compatible with such a liquid environment in the sensor. During a typical time-dependent detection process for quantifying the binding reaction kinetics, the sensing FET is electrically biased and constantly exposed to the analyte solution. The process applies a gate voltage (V_G) to bias the FET to the linear regime of the transfer characteristic to obtain a high sensitivity as well as a consistent sensor response behavior,[4,7] and a drain-source voltage (V_{DS}) for driving the sensing channel current (I_{DS}). Such continuous electrical stresses in the liquid reagent environment can result in undesirable leakage currents flowing to electrodes, generate high-level electronic noises and false sensor responses, and even electrochemically damage the sensor. It should be noted that even the FET sensor coated with an insulating layer (e.g., TiO$_2$, SiO$_2$, or Al$_2$O$_3$ layers) can hardly survive in a long continuous time-dependent detection process (e.g., several hours for fM-level quantification) because of the electric-field-enhanced permeation of reactive ions into the insulating layer.[9,10] The analyte solutions with different ionic strengths also cause different degrees of the screening effect to the electrostatic interaction between target molecules and the sensing channel, resulting in inconsistent sensor response signals. Such a screening effect also degrades the biodetection sensitivity of the sensor.[11−14] Another serious issue associated with TMDC-based FET sensors is the hysteretic behavior of the transfer characteristics of such sensors, which is attributed to the gate-modulated charges trapped at TMDC/dielectric interfaces.[15] Such a hysteretic behavior makes the I_{DS} value measured under a given V_G highly

dependent on the sweep range, sweep direction, sweep time and loading history of V_G biases, therefore resulting in inconsistent sensor readings. To rule out such uncertainty of sensor readings due to the hysteresis effect, ones need to measure the whole transfer characteristic curves (i.e., I_{DS}−V_G curves) by sweeping V_G along both positive and negative directions, which is similar to the way for characterizing a charge-controlled FET memory.[16−18] However, this electrical measurement process is not applicable during a continuous time-dependent detection process. Another expedient solution is to constantly bias the FET sensor to the linear (or highly conductive) transport regime, where the hysteresis-induced indeterminacy of I_{DS} values is much smaller than that in the subthreshold regime. However, as discussed above, such a constantly applied gate bias can easily damage the sensor. In addition, during a continuous time-dependent detection process, the nonspecific adsorption of untargeted molecules on the FET sensing channel can also generate false signals. All of these issues seriously limit the applicability of TMDC-based FET biosensors for realizing rapid, highly specific biomolecule quantification based on time-dependent sensor response signals or nonequilibrium-state sensor responses.

In this paper, we present a cyclewise time-dependent biodetection method for operating MoS$_2$-based FET biosensors. Such a cyclewise process alternatively sets the FET sensor into incubation, flushing, and electrical measurement steps and therefore avoids the liquid-solution-induced electrochemical damage, screening, and nonspecific adsorption to the sensor. This method can also rule out the indeterminacy of sensor readings due to the hysteretic behaviors of TMDC FETs. This cyclewise detection method in combination with the superior sensitivity and limit-of-detection (LOD) of TMDC-based biosensors enables rapid, low-noise, and highly specific biomolecule quantification with fM-level LODs even in

complex analyte solutions. In this work, we have experimentally characterized time-dependent sensor responses associated with the reaction kinetics of streptavidin−biotin and Interleukin 1-beta (IL-1β)-antibody bindings and demonstrated fM-level streptavidin and IL-1β quantifications in pure as well as complex solutions (e.g., serum and saliva) with detection limit of ∼1 fM and total detection time less than 23 min.

■ EXPERIMENTAL SECTION

Fabrication of MoS$_2$ FET Biosensors. The MoS$_2$ FETs are constructed onto p$^+$-Si substrates with 300 nm thermally grown SiO$_2$ layers using our previously published nanoprinting method.[3] The 300 nm-thick SiO$_2$ layers serve as back-gate dielectrics and also enable a simple color coding method to quickly identify and locate the few-layer MoS$_2$ flakes with suitable thicknesses.[19] The thicknesses of printed few-layer-MoS$_2$ FET channels are specifically controlled to be 5−10 nm. Such MoS$_2$ channel thicknesses can result in the optimal field-effect mobility and On/Off ratio values for the FETs.[20−22] The p$^+$-Si substrates serve as the back gates (G). Ti (10 nm)/Au (50 nm) drain (D) and source (S) contacts to the MoS$_2$ channels are fabricated using photolithography. The channel length and width of as-fabricated MoS$_2$ FETs are ∼5 and ∼15 μm, respectively. Electrical measurements are performed using an HP-4145B semiconductor parameter analyzer, connected to a Lakeshore probe station. Each of the MoS$_2$ FETs biosensors is attached with a polydimethylsiloxane (PDMS) block bearing a microfluidic channel (10 mm in length, 200 μm in width, 50 μm in height), as illustrated in Figure 1a. A motorized syringe pump is used to drive the reagent flows into and out of the microfluidic structure through an tubing kit (diameter: 0.75 mm).

Functionalization of MoS$_2$ FET Biosensors and Biodetection Processes. Before functionalization, the as-fabricated MoS$_2$ FET biosensor is incubated in 5% (3-aminopropyl)triethoxysilane (APTES) in ethanol for 1 h. In the case of IL-1β antibody functionalization, an additional 5% glutaldehyde in phosphate-buffered saline (PBS) is used to incubate the FET sensor for another 2 h. After the incubation process, the sensor is rinsed with deionized (DI) water and blown dry by using an air gun. Then 50 μg/mL NHS-biotin (for detecting streptavidin) or 50 μg/mL IL-1β antibody (for detecting IL-1β) in PBS is subsequently incubated on the MoS$_2$ FET channel area for 30 min. Before the biodetection process, a PDMS microfluidic structure is attached on top of the FET sensor. A pair of inlet/outlet tubes is connected with this microfluidic structure and used to deliver a time-sequenced series of reagent fluids, including analyte solutions of streptavidin or IL-1β, pure buffers, DI water flows, and air flows. Specifically, liquid solution flows, i.e., analyte and buffer solution flows, are driven into the sensor by using a syringe pump; the air flow for drying the sensor is generated by connecting the outlet tube with a vacuum supply nozzle and letting the inlet tube open to air. During a biodetection cycle, the time durations for incubation in the analyte solution, flushing using pure buffer and DI water, drying using air flow, and electrical measurement are set to 10 min (or 5 min), ∼5, ∼20, and ∼20 s, respectively.

■ RESULT AND DISCUSSION

Figure 1a illustrates the MoS$_2$-based FET biosensor, which is integrated with a polydimethylsiloxane (PDMS)-based microfluidic channel. The sensing FET channel made from a few-layer MoS$_2$ flake is functionalized with specific antibody receptors for detecting the target molecules in the analyte solution. In this work, MoS$_2$ FET channels are functionalized with either biotin or IL-1β antibody receptors for detecting streptavidin or IL-1β molecules presented in pure and complex solutions, as illustrated in Figure 1b and c. The fabrication and functionalization of such integrated biosensors are described in the Experimental Section.

Figure S-1 in the Supporting Information illustrates the cyclewise biodetection process for operating a MoS$_2$ FET

sensor. During this process, the microfluidic structure is operated to deliver a series of time-sequenced reagent fluids to the sensing FET channel and periodically set the sensor into four assay-cycle stages, including (i) incubation of the sensing channel in the analyte solution containing target molecules for a short but deterministic duration (typically 5−10 min), (ii) flushing the sensing channel using pure buffer and DI water to eliminate unreacted target molecules and untargeted background molecules, (iii) drying the sensing channel using an air flow, and (iv) electrically measuring, under such a dry condition, the transfer characteristics (i.e., I_{DS}−V_G characteristic curves) of the sensing FET by sweeping V_G along both positive and negative directions. Repetitive operation with multiple such incubation-flushing-drying-measurement (IFDM) cycles can acquire a time-dependent sensor response signal associated with the reaction kinetics of analyte-receptor binding. More details about this IFDM cyclewise method are described in the Experimental Section.

Figure S-2a shows the scanning electron micrograph (SEM) of as-printed few-layer-MoS$_2$ FET channels. Each of the printed channels is associated with a pair of Ti/Au align-marks, which are used for locating the FET channel specifically selected for making a working biosensor. Figure S-2b displays the optical micrograph of a representative FET biosensor consisting of a few-layer MoS$_2$ channel (thickness ∼5 nm), and a pair of metallic drain/source (D/S) contacts (10 nm Ti/50 nm Au). The FET channel length and width are 5 and 15 μm, respectively. Figure S-2c shows the photograph of a MoS$_2$ FET sensor integrated with a PDMS microfluidic structure. This microfluidic structure is connected with a syringe pump. We can operate this pump/tubing system to deliver a time-sequenced series of reagent fluids to the FET sensing channel for performing IFDM detection cycles.

Figure S-3 in the Supporting Information shows the time-dependent transfer characteristics (i.e., I_{DS}−V_G characteristics) measured from a set of MoS$_2$ FET sensors using the cyclewise method discussed above. Each of these sensors was subjected to a different concentration of streptavidin (Figure S-3 show the results for different streptavidin concentrations $n_{streptavidin}$ = 0, 1, 4, 20, 100, and 300 fM). Specifically, this set of MoS$_2$ sensors were fabricated in the same batch using our previously published nanoprinting method that can enable production of multiple few-layer MoS$_2$ FETs with a high device-to-device consistency in their transport characteristics.[3] Here, for each IFDM cycle, the incubation time (T_i) was set to 10 min. In the following discussion, the sensor responses are analyzed as a function of accumulative incubation time (t), which is defined as $t = nT_i$ (here, n is the number of already performed IFDM cycles). In this experiment, the transfer curves of each MoS$_2$ sensor were acquired at a series of IFDM cycles with t values ranging from 0 to 110 min (i.e., 11 IFDM cycles for a detection course). As shown in Figure S-3, for each FET sensor in response to a specific streptavidin concentration, the linear regime of its transfer curve exhibits an evolutionary reduction of the FET transconductance (i.e., $g_m = \frac{\partial I_{DS}}{\partial V_G}$ in the linear regime of the transfer curve) or the I_{DS} measured at given V_G and V_{DS} with increasing the accumulative incubation time t. Such a reduction behavior of g_m and I_{DS} values is attributed to the net effect of target-molecule-induced electrostatic doping and target-molecule-induced surface scattering of carriers.[6,7] In addition, the reduction rate and range of the g_m and I_{DS} values in the linear regime of the transfer curve become larger with

enhancing the streptavidin concentration, as displayed in Figure S-3. This is attributed to the fact that the binding rate of biotin−streptavidin pairs increases with increasing streptavidin concentration, and the final occupancy of biotin receptors at the equilibrium state of the biotin−streptavidin binding reaction becomes larger at the higher streptavidin concentration.[23] Although the $n_{streptavidin} = 0$ case (Figure S-3a) is not expected to result in any specific binding reaction, the t-dependent I_{DS}−V_G curves of the FET sensor still exhibit an observable reduction of the g_m (or I_{DS}) in the linear regime with increasing t. This indicates that the pure buffer solution still results in moderate nonspecific absorption of ions or molecules on the MoS_2 channel. Currently, we have not fully understood the mechanism of such nonspecific absorption, but temporarily attributed it to the slow reaction between the crystal defects on the MoS_2 channel and the ions in the buffered solution.[24]

Figure S-3b specifically shows the t-dependent I_{DS}−V_G curves measured at $n_{streptavidin} = 1$ fM. For this sensor, at each IFDM cycle (i.e., at each t point), two I_{DS}−V_G curves were acquired with different V_G sweep directions. One was measured with positive V_G sweep direction (i.e., from −100 to 100 V, "positively-scanned curve"), and the other was measured with negative V_G sweep direction (i.e., from 100 to −100 V, "negatively scanned curve"). Figure S-3b shows that the MoS_2 sensor exhibits a prominent hysteretic behavior in its transfer characteristics. Such a hysteretic behavior is attributed to the V_G-modulated charge trapped at MoS_2/dielectric interfaces or moisture molecules.[15,25] Although both sets of the positively and negatively scanned I_{DS}−V_G curves exhibit similar g_m/I_{DS}-reduced response behaviors with increasing t, the observed hysteresis of I_{DS}−V_G curves could result in undesirable indeterminacy of sensor readings. Specifically, to quantify the time-dependent reaction kinetics of an analyte−receptor binding reaction, the I_{DS} values measured at given V_G or the g_m values in the linear regime of the I_{DS}−V_G curves are captured and plotted as a function of accumulative incubation time t. The hysteretic effect makes the acquired I_{DS}−t or g_m−t response curves highly dependent on the loading history of V_G biases, resulting in serious inaccuracy of sensor readings for real-time biomolecule quantification. As implied by Figure S-3b, a solution to minimize the hysteresis-induced indeterminacy of sensor readings is to use the I_{DS} data measured in the highly conductive regime of I_{DS}−V_G curves (e.g., $V_G = 100$ V for our n-type MoS_2 FETs) as the sensor response signals. The I_{DS}−t response signals captured at $V_G = 100$ V is expected to enable reliable quantification of the time-dependent kinetics of analyte-receptor binding reactions with the minimal hysteresis-induced sensor inaccuracy. Here, it should be noted that the IFDM cyclewise method is highly compatible with the acquisition of I_{DS}−t response signals at $V_G = 100$ V, because in an IFDM cycle, the electrical measurement of I_{DS}−V_G curves in the V_G range of −100 to 100 V is separated from the incubation in the liquid solution, which can effectively avoid the large-bias-induced electrochemical damage to the FET. This is an advantage of the IFDM cyclewise method in minimizing or eliminating hysteresis-induced inaccuracy of sensor readings.

As discussed for Figure S-3, I_{DS}−t response signals can be captured from the highly conductive n-type branches of the I_{DS}−V_G curves of MoS_2 FET sensors. To further minimize the device-to-device variation in captured I_{DS} values, we use the relative percentage change in I_{DS} (i.e., $S = 100\% \times [I_{DS}(t) - I_{DS}(t = 0)]/I_{DS}(t = 0)$) with respect to the accumulative incubation time (t) as a calibrated time-dependent sensor

response signal. Here, S can also serve as the biodetection sensitivity. Figure 2a plots the S−t response curves correspond-
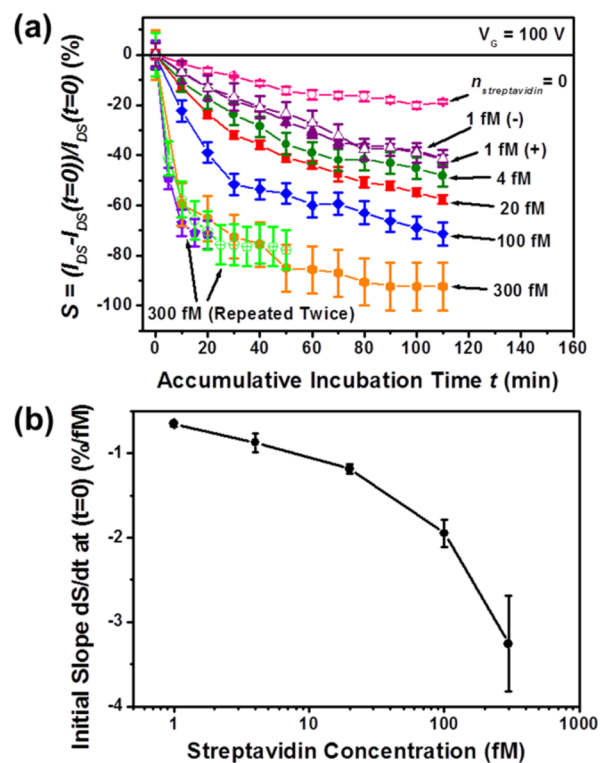

Figure 2. (a) S−t response curves measured at different streptavidin concentrations ($n_{streptavidin} = 0, 1, 4, 20, 100,$ and 300 fM), which are captured from the t-dependent I_{DS}−V_G curves of a set of MoS_2 sensors. (b) dS/dt−$n_{streptavidin}$ curve extracted from the S−t response curves.

ing to different streptavidin concentrations ($n_{streptavidin} = 0, 1, 4, 20,$ and 300 fM), which were captured from the corresponding t-dependent I_{DS}−V_G curves displayed in Figure S-3. The nonflat S−t curve at $n_{streptavidin} = 0$ serves as the biodetection baseline. The S−t curve measured at $n_{streptavidin} = 1$ fM can be well resolved from this baseline. This demonstrates that the MoS_2 FET sensors operated by the IFDM cyclewise method can enable a LOD of at least 1 fM for streptavidin detection. In Figure 2a, the S−t response curves labeled with "1 fM (+)" and "1 fM (−)" are captured from the positively and negatively scanned t-dependent I_{DS}−V_G curves shown in Figure S-3b (captured at $V_G = 100$ V), respectively. These two S−t response curves are highly consistent with each other regardless of the scanning direction (or the loading history of V_G-modulated charges). This further demonstrates that the IFDM cyclewise method can generate unambiguous time-dependent sensor response signals for biomolecule quantification and rule out the indeterminacy of sensor readings due to the hysteresis of the transfer characteristics of TMDC-based FETs.

We further extracted derived sensor response parameters from the measured S−t response curves to obtain a standard curve (i.e., calibrated sensor response (R) versus analyte concentration (n) curve) for enabling rapid biomolecule quantification. Figure 2a shows that within an accumulative incubation time (t) of ~2 h, the S−t response curves measured at $n_{streptavidin} < 300$ fM do not fully saturate to the S values corresponding to the equilibrium states of the binding reaction processes. This means that the sensor response quantities

measured at the equilibrium states are not suitable for rapid femtomolar-level biomolecule quantification, because even for the analyte-receptor pair with a strong affinity (e.g., streptavidin–biotin pair), it still takes several hours for the binding reaction to reach to the equilibrium state. Figure 2a also shows that the initial slopes of S–t response curves exhibit a strong dependence on streptavidin concentrations and can be exploited for rapid streptavidin quantification. The determination of such initial slopes of S–t curves does not need a long accumulative incubation time until the binding reaction reaches to the equilibrium state. Therefore, the initial slope of an S–t curve (i.e., dS/dt at $t \sim 0$) can serve as a derived sensor response quantity for enabling rapid biomolecule quantification. Here, the specific dS/dt value is extracted from the S–t response curve through linearly fitting the S data measured within the first three IFDM cycles (typically, the accumulative incubation time is ~20 min, and the total assay time is less than 23 min). Figure 2 (b) plots the dS/dt–$n_{\text{streptavidin}}$ curve extracted from the S–t response curves shown in Figure 2a. Such a dS/dt–$n_{\text{streptavidin}}$ curve can serve as a standard curve for rapid streptavidin quantification at femtomolar levels. It should be noted that the dS/dt value for $n = 0$ (i.e., $-0.31 \pm 0.01\%/$fM) is not shown in semilogarithmic Figure 2b. The dS/dt value for $n = 1$ fM (i.e., $-0.65 \pm 0.03\%/$fM) is well distinct from this baseline value.

To evaluate the repeatability of biomolecule quantification based on initial slopes of S–t response curves, another two MoS$_2$ FET sensors were used to repeat the cyclewise detection course at $n_{\text{streptavidin}} = 300$ fM and generate another two S–t response curves, which are also plotted in Figure 2a. The corresponding t-dependent I_{DS}–V_{G} curves of these two sensors are shown in Figure S-4 in the Supporting Information. All three S–t response curves for $n_{\text{streptavidin}} = 300$ fM are consistent with each other. Especially, their initial slopes are very close (the relative standard deviation is ~16%) and can be unambiguously associated with 300fM streptavidin. In addition, for these two repeated courses, the incubation time (T_i) in an IFDM cycle is 5 min. As shown in Figure 2a, the S–t response curves measured by these two sensors at $T_i = 5$ min are consistent with that measured at $T_i = 10$ min. This result also shows that the variation of the IFDM cycle period in the range of 5–10 min does not significantly affect the resulted t-dependent sensor response signals.

We further used our MoS$_2$ FET sensors and the cyclewise method for investigating the quantification of other clinical biomarkers, which usually exhibit a much weaker affinity to their receptors in comparison with streptavidin. Here, we demonstrated Interleukin 1beta (IL-1β) quantification. IL-1β is a cytokine protein and serves as an important mediator of the inflammatory response.[26–29] It is associated with many cellular activities, including proliferation, differentiation, and apoptosis.[30–32] IL-1β has a relatively weak affinity to its antibody in comparison with streptavidin (i.e., the affinity constant for the streptavidin–biotin pair $K_{\text{D,streptavidin}} \sim 10^{-14}$ M, and that of the IL-1β-antibody $K_{\text{D,IL-1}\beta} \sim 10^{-9}$ M (or 1 nM)). Therefore, rapid fM-level IL-1β quantification is still a challenge (note that IL-1β quantification with LOD of ~10 fM can be realized by using advanced enzyme-linked immunosorbent assays (ELISAs), but such assays still need very long processing times).[33–35]

Figure S-5 displays the t-dependent I_{DS}–V_{G} characteristic curves measured from a set of six MoS$_2$ FET sensors, which were subjected to a set of IL-1β solutions with different IL-1β concentrations (i.e., $n_{\text{IL-1}\beta} = 0$, 1, 4, 20, 100, and 500 fM),

respectively. From these I_{DS}–V_{G} curves, the corresponding S–t response curves were extracted at $V_{\text{G}} = 100$ V and plotted in Figure 3a. The method for processing the sensing data for IL-
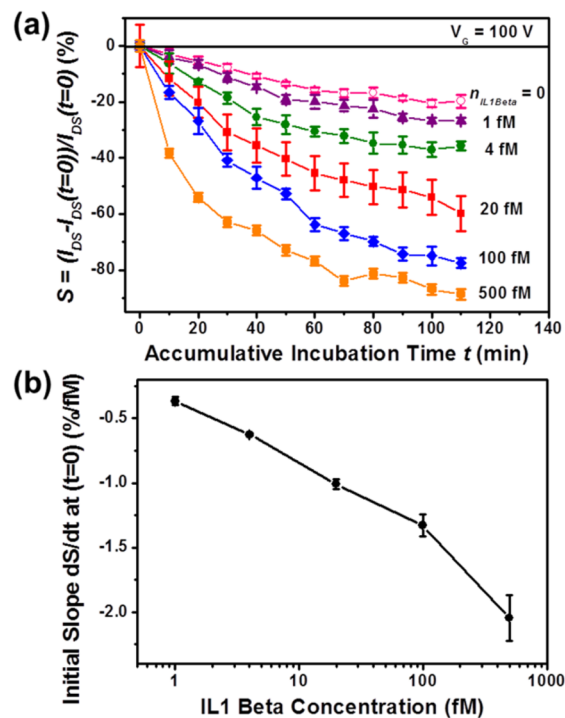

Figure 3. (a) S–t response curves measured at different IL-1β concentrations ($n_{\text{IL-1}\beta} = 0$, 1, 4, 20, 100, and 500 fM), which are captured from the t-dependent I_{DS}–V_{G} curves. (b) dS/dt–$n_{\text{IL-1}\beta}$ curve extracted from the S–t response curves.

1β quantification is the same as that for streptavidin quantification. Here, the S–t response curve for $n_{\text{IL-1}\beta} = 0$ is still not flat but is highly consistent with that for $n_{\text{streptavidin}} = 0$. This further indicates that such a zero-concentration S–t response curve can serve as a generic baseline for quantification of different target molecules in the same solvent. Figure 3a shows that the S–t response curve measured at $n_{\text{IL-1}\beta} = 1$ fM is clearly resolvable from the nonflat baseline measured at $n_{\text{IL-1}\beta} = 0$. This indicates that our MoS$_2$ FET biosensors in combination with the IFDM cyclewise method can result in a LOD of ~1 fM for IL-1β quantification. As discussed for streptavidin quantification, the initial slopes of the S–t response curves shown in Figure 3a can be also used as a derived response quantity for enabling rapid IL-1β quantification. Figure 3b shows the extracted dS/dt data plotted as a function of the IL-1β concentrations ($n_{\text{IL-1}\beta}$). Here, the dS/dt value for $n = 1$ fM (i.e., $-0.37 \pm 0.03\%/$fM) is well distinct from that for $n = 0$ (i.e., $-0.26 \pm 0.02\%/$fM). Similar to the case for streptavidin quantification, to unambiguously determine the dS/dt values for IL-1β quantification, the minimum incubation time is about 20 min, and the corresponding total assay time is about 23 min. Therefore, this work has further demonstrated that the MoS$_2$ FET biosensors operated using the IFDM cyclewise method can enable rapid femtomolar-level quantification of IL-1β and other biomolecules with relatively weak affinities (i.e., nM-level K_{D} values) to their receptors. Here, IL-1β and streptavidin molecules have very close isoelectric point values (~7) in a PBS solution.[36,37] Therefore, the effect of their charges on their resulted sensor responses is not expected to be significant. The

difference between their resulted sensor responses is attributed to their different affinities to the receptors. Furthermore, the current IFDM cycle period is 5−10 min, which is limited by our current microfluidic pumping system. Therefore, we set the total incubation time to be ∼20 min to ensure that at least three data points could be obtained to determine the slope values of S−t curves. Therefore, the total incubation time is currently not limited by analyte-receptor pairs but temporarily limited by the flow rate of our current microfluidic system.

In another experiment, we characterized two MoS$_2$ FET sensors for a direct comparison of the time-dependent response signals measured using the IFDM cyclewise method and the regular continuous detection method. Figure 4 shows these two
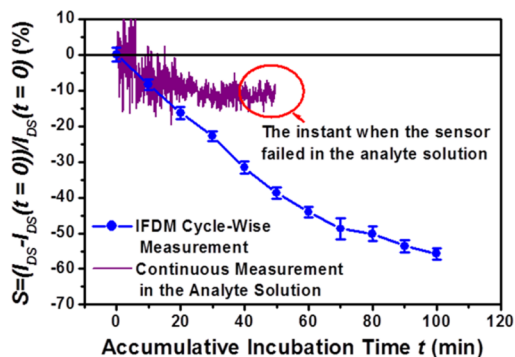

Figure 4. Comparison between the S−t response signals obtained using the IFDM cyclewise method (solid circles) and the regular continuous detection method (solid line).

sensors' responses to the same pure 30 fM streptavidin solution. Specifically, one of the sensors was operated by using the IFDM cyclewise method (T_i = 10 min). The solid circles in Figure 4 represent the calibrated S−t response signal measured by this sensor. Another sensor was used to continuously measure the electrical signal associated with the time-dependent reaction kinetics of biotin−streptavidin binding. In particular, this sensor was continuously biased with a back-gate voltage (V_G) of 100 V and a drain-source voltage (V_{DS}) of 1 V. Since the 30 fM streptavidin solution was introduced into the sensor, the instant I_{DS} signal had been being continuously recorded as a function of t. This continuous $I_{DS} − t$ signal was also calibrated into the signal of t-dependent relative change in I_{DS} (i.e., the S−t signal), which was also plotted in Figure 4. In comparison with this S−t signal obtained using the continuous detection method, the S−t signal obtained using the IFDM cyclewise method exhibits the larger signal magnitude (i.e., the higher sensitivity) and the smaller relative error of the signal magnitude (i.e., the higher signal-to-noise ratio) at a given accumulative incubation time. The relatively weaker magnitude of the S−t signal obtained using the continuous method is attributed to the Debye screening effect of the liquid solution, which can weaken the electrostatic coupling between the charges of target molecules and the FET channel, resulting in the lower sensitivity.[11−14] The IFDM cyclewise method can address this issue through physically isolating the incubation and measurement stages during an IFDM cycle. This cyclewise method can also eliminate the electrical noise from the liquid solution and therefore result in the lower LOD. Additionally, as shown in Figure 4, the MoS$_2$ sensor operated using the continuous method failed at $t ∼ 50$ min.

Our other TMDC FET sensors, when operated using the continuous method, also usually fail within 1 h of the operation. Here, the failure of a MoS$_2$ sensor means that the MoS$_2$ channel is electrochemically broken into isolated pieces and the I_{DS} signal drops to undetectable levels. This is attributed to the long-time exposure of the MoS$_2$ channel to electrical stress and liquid environment, which can result in an electrochemical corrosion in MoS$_2$ layers. However, the similar TMDC sensors, if operated using the cyclewise method, can properly work for several hours without damage. Therefore, this comparison work indicates that the TMDC FET sensors operated using the IFDM cyclewise method exhibit the better durability, the higher sensitivity, and the higher signal-to-noise ratio than those operated using the continuous detection method.

To evaluate the detection specificity of the MoS$_2$ biosensors operated by the cyclewise method and the effect of complex solutions on the detection results, we further performed two experiments to study the time-dependent sensor responses to biotin−streptavidin and IL-1β-antibody binding reactions in various solution backgrounds. In the first experiment, we fabricated three MoS$_2$ FET biosensors in the same batch. One of them (sensors #1) was used to quantify 20 fM streptavidin in a pure solution. The other two sensors (sensors #2 and #3) were used to quantify 20 fM streptavidin in a solution that also contained 60 fM tumor necrosis factor alpha (TNF-α). Figure S-6 in the Supporting Information shows the t-dependent I_{DS}−V_G curves of these three MoS$_2$ FET sensors. Figure S-7 plots three S−t response curves extracted from the t-dependent I_{DS}−V_G curves of these three MoS$_2$ sensors. These three S−t response curves are highly consistent with each other. This indicates that the presence of 60 fM TNF-α in the analyte solution does not noticeably affect the t-dependent sensor responses to 20 fM streptavidin.

In the second experiment, four MoS$_2$ FET biosensors were used to quantify 20 fM IL-1β in a pure solution (sensor #1), a solution also containing 100 fM TNF-α (sensor #2), serum (sensor #3), and saliva (sensor #4), respectively. The serum matrix used here was purchased from Merck KGaA, Inc. and diluted by 20 times in DI water. It contains 0.08% sodium azide. The saliva used here was collected from healthy human donors using reported drooling method.[38] The as-pooled saliva was diluted in DI water by 10 times. Figure S-8 in the Supporting Information shows the t-dependent I_{DS}−V_G curves of these four MoS$_2$ FET sensors, which were measured using IFDM cycles (T_i = 10 min). Figure S-9 in the Supporting Information plots the S−t response curves extracted from the t-dependent I_{DS}−V_G curves of these four MoS$_2$ sensors. All of these S−t signals in response to 20 fM IL-1β in different solution backgrounds are consistent with each other. This good consistency further demonstrates that the reliable t-dependent sensor responses to target analyte molecules can be acquired regardless of the different solution backgrounds, and the complex protein backgrounds in serum and saliva do not significantly affect the t-dependent sensor readings associated with the specific concentrations of target molecules. The slight difference among these S−t curves in Figures S-7 and S-9 is attributed to the slight sensor-to-sensor variation in transport characteristics. These two comparison experiments have demonstrated that the MoS$_2$ FET biosensors operated using the IFDM cyclewise method exhibit a high biodetection specificity. This is attributed to the flushing step in an IFDM cycle, which can effectively remove nonspecifically adsorbed molecules from the FET sensing channel, therefore minimizing

the false sensor responses. Furthermore, two-dimensional MoS_2 or other TMDC surfaces usually have a very low friction coefficient and exhibit very low adhesion to other materials, which is expected to make the flushing of nonspecifically adsorbed molecules on TMDC FET channels much easier than that on the FET channels made from conventional semi-conductors.[39]

We also measured the $S-t$ responses to different IL-1β concentrations presented in serum. Figures S-10 and S-11a in the Supporting Information display t-dependent $I_{DS}-V_G$ characteristic curves and derived $S-t$ response curves, respectively. Figure S-11b plots the $dS/dt-n_{IL-1\beta}$ standard curve extracted from the $S-t$ curves in Figure S-11a, which is compared to the standard curve measured from the IL-1β molecules presented in the pure solvent. Figure S-11b further shows that the standard curve obtained from a complex solution is basically consistent with that obtained from the pure solution. The slight difference between them is attributed to the slight sensor-to-sensor variation in their transport character-istics or the slightly different baselines caused by the different solution backgrounds. As a comparison, we also obtained a correlation curve for IL-1β quantification in serum using standard ELISA. Figure S-12a and b in the Supporting Information plot such an ELISA-measured correlation curve in linear and semilogarithmic scales, respectively. Figure S-12c displays a photograph of the ELISA wells used for obtaining the correlation curve. Figure S-12b shows that, for IL-1β concentrations less than 1 pM, the ELISA signals can be hardly resolved from the zero concentration baseline, and the LOD of the standard ELISA for IL-1β quantification in serum is estimated to be ~1 pM. Therefore, our cyclewise detection method using MoS_2 FETs results in a much lower LOD in comparison with the standard ELISA.

Finally, we provide a comparison of the LOD and incubation time parameters obtained by the presented IFDM cyclewise method based on MoS_2 sensors, other representative FET biosensors, and advanced ELISA, as shown in Table S-1 in the Supporting Information. In comparison with previously reported FET biosensors made from graphene layers,[40] Si nanowires,[23,41] and MoS_2 layers,[1,2] our MoS_2 sensors operated by the cyclewise detection method enable a lower LOD for quantifying low-abundant biomolecules. For femtomolar-level IL-1β quantification, our IFDM cyclewise method can result in a much shorter required incubation time in comparison with advanced ELISA.[33−35]

CONCLUSION

We established a cyclewise approach for operating MoS_2 FET biosensors. This approach enabled rapid, low-noise, highly specific biomolecule quantification and analyte−receptor bind-ing kinetics analysis. Combined with the high sensitivity and low detection limit of MoS_2 biosensors, this cyclewise detection method can realize rapid biomolecule quantification at femtomolar levels. In this work, we have demonstrated the quantification of streptavidin and IL-1β suspended in pure and complex solutions with a detection limit of ~1 fM and a total assay time less than 23 min. This work leverages the superior electronic properties of emerging layered materials for biosensing applications and advances the sensor operation technology toward realizing fast biomolecule quantification at femtomolar levels.

ASSOCIATED CONTENT

Supporting Information

The Supporting Information is available free of charge on the ACS Publications website at DOI: 10.1021/acssen-sors.6b00795.

> Biosensor structure and method; t-dependent $I_{DS}-V_G$ curves measured at different streptavidin concentrations; $I_{DS}-V_G$ curves measured at 300 fM; $I_{DS}-V_G$ curves measured at different IL-1β concentrations; responses in various solutions; $I_{DS}-V_G$ curves measured in serum; correlation curves for IL-1β in serum; comparison among the cyclewise method, other FET biosensors, and ELISA (PDF)

AUTHOR INFORMATION

Corresponding Author
*E-mail: xiaoganl@umich.edu.

ORCID
Xiaogan Liang: 0000-0002-7390-9130

Author Contributions
§B.R. and H.N. contributed equally. The manuscript was written through contributions of all authors.

Notes
The authors declare no competing financial interest.

ABBREVIATIONS

DI, deionized; FET, field-effect transistors; LOD, limit-of-detection; TMDC, transition metal dichalcogenide; PDMS, polydimethylsiloxane; SEM, scanning electron micrograph

REFERENCES

(1) Wang, L.; Wang, Y.; Wong, J. I.; Palacios, T.; Kong, J.; Yang, H. Y. Functionalized MoS_2 Nanosheet-Based Field-Effect Biosensor for Label-Free Sensitive Detection of Cancer Marker Proteins in Solution. Small 2014, 10, 1101−1105.

(2) Sarkar, D.; Liu, W.; Xie, X. J.; Anselmo, A. C.; Mitragotri, S.; Banerjee, K. MoS_2 Field-Effect Transistor for Next-Generation Label-Free Biosensors. ACS Nano 2014, 8, 3992−4003.

(3) Chen, M.; Nam, H.; Rokni, H.; Wi, S.; Yoon, J. S.; Chen, P.; Kurabayashi, K.; Lu, W.; Liang, X. Nanoimprint-Assisted Shear Exfoliation (NASE) for Producing Multilayer MoS_2 Structures as Field-Effect Transistor Channel Arrays. ACS Nano 2015, 9, 8773−8785.

(4) Nam, H.; Oh, B. R.; Chen, P. Y.; Chen, M. K.; Wi, S. J.; Wan, W. J.; Kurabayashi, K.; Liang, X. G. Multiple MoS_2 Transistors for Sensing Molecule Interaction Kinetics. Sci. Rep. 2015, 5, 10546.

(5) Lee, J.; Dak, P.; Lee, Y.; Park, H.; Choi, W.; Alam, M. A.; Kim, S. Two-Dimensional Layered MoS_2 Biosensors Enable Highly Sensitive Detection of Biomolecules. Sci. Rep. 2014, 4, 7352.

(6) Nam, H.; Oh, B. R.; Chen, P.; Yoon, J. S.; Wi, S.; Chen, M. K.; Kurabayashi, K.; Liang, X. Two Different Device Physics Principles for Operating MoS_2 Transistor Biosensors with Femtomolar-Level Detection Limits. Appl. Phys. Lett. 2015, 107, 012105.

(7) Nam, H.; Oh, B. R.; Chen, M. K.; Wi, S.; Li, D.; Kurabayashi, K.; Liang, X. G. Fabrication and Comparison of MoS_2 and WSe_2 Field-Effect Transistor Biosensors. J. Vac. Sci. Technol., B: Nanotechnol. Microelectron.: Mater., Process., Meas., Phenom. 2015, 33, 06FG01.

(8) Luchansky, M. S.; Bailey, R. C. Rapid, Multiparameter Profiling of Cellular Secretion Using Silicon Photonic Microring Resonator Arrays. J. Am. Chem. Soc. 2011, 133, 20500−20506.

(9) Atkinson, A. Growth of NiO and SiO$_2$ Thin-Films. *Philos. Mag. B* **1987**, *55*, 637−650.

(10) Sarantaridis, D.; Atkinson, A. Redox Cycling of Ni-Based Solid Oxide Fuel Cell Anodes: A Review. *Fuel Cells* **2007**, *7*, 246−258.

(11) Kulkarni, G. S.; Zhong, Z. H. Detection beyond the Debye Screening Length in a High-Frequency Nanoelectronic Biosensor. *Nano Lett.* **2012**, *12*, 719−723.

(12) Lee, W. H.; Lee, J. M.; Uhm, M.; Lee, J.; Kim, K. R.; Choi, S. J.; Kim, D. M.; Jeong, Y. J.; Kim, D. H. Characterization and Capacitive Modeling of Target Concentration-Dependent Subthreshold Swing in Silicon Nanoribbon Biosensors. *IEEE Electron Device Lett.* **2014**, *35*, 587−589.

(13) Shoorideh, K.; Chui, C. O. Optimization of the Sensitivity of FET-Based Biosensors via Biasing and Surface Charge Engineering. *IEEE Trans. Electron Devices* **2012**, *59*, 3104−3110.

(14) Shoorideh, K.; Chui, C. O. On the Origin of Enhanced Sensitivity in Nanoscale FET-Based Biosensors. *Proc. Natl. Acad. Sci. U. S. A.* **2014**, *111*, 5111−5116.

(15) Late, D. J.; Liu, B.; Matte, H. S. S. R.; Dravid, V. P.; Rao, C. N. R. Hysteresis in Single-Layer MoS$_2$ Field Effect Transistors. *ACS Nano* **2012**, *6*, 5635−5641.

(16) Choi, M. S.; Lee, G. H.; Yu, Y. J.; Lee, D. Y.; Lee, S. H.; Kim, P.; Hone, J.; Yoo, W. J. Controlled Charge Trapping by Molybdenum Disulphide and Graphene in Ultrathin Heterostructured Memory Devices. *Nat. Commun.* **2013**, *4*, 1624.

(17) Zhou, Y.; Han, S. T.; Sonar, P.; Roy, V. A. L. Nonvolatile Multilevel Data Storage Memory Device from Controlled Ambipolar Charge Trapping Mechanism. *Sci. Rep.* **2013**, *3*, 2319.

(18) Chen, M. K.; Nam, H.; Wi, S.; Priessnitz, G.; Gunawan, I. M.; Liang, X. G. Multibit Data Storage States Formed in Plasma-Treated MoS$_2$ Transistors. *ACS Nano* **2014**, *8*, 4023−4032.

(19) Zhang, Y. J.; Ye, J. T.; Yomogida, Y.; Takenobu, T.; Iwasa, Y. Formation of a Stable p−n Junction in a Liquid-Gated MoS$_2$ Ambipolar Transistor. *Nano Lett.* **2013**, *13*, 3023−3028.

(20) Bao, W. Z.; Cai, X. H.; Kim, D.; Sridhara, K.; Fuhrer, M. S. High Mobility Ambipolar MoS$_2$ Field-Effect Transistors: Substrate and Dielectric Effects. *Appl. Phys. Lett.* **2013**, *102*, 042104.

(21) Chen, M.; Nam, H.; Wi, S.; Lian, J.; Ren, X.; Bian, L. F.; Lu, S.; Liang, X. G. Stable Few-Layer MoS$_2$ Diodes Formed by Plasma-Assisted Doping. *Appl. Phys. Lett.* **2013**, *103*, 142110.

(22) Nam, H.; Wi, S.; Rokni, H.; Chen, M. K.; Priessnitz, G.; Lu, W.; Liang, X. G. MoS$_2$ Transistors Fabricated *via* Plasma-Assisted Nanoprinting of Few-Layer MoS$_2$ Flakes into Large-Area Arrays. *ACS Nano* **2013**, *7*, 5870−5881.

(23) Duan, X. X.; Li, Y.; Rajan, N. K.; Routenberg, D. A.; Modis, Y.; Reed, M. A. Quantification of The Affinities and Kinetics of Protein Interactions Using Silicon Nanowire Biosensors. *Nat. Nanotechnol.* **2012**, *7*, 401−407.

(24) Li, H.; Du, M.; Mleczko, M. J.; Koh, A. L.; Nishi, Y.; Pop, E.; Bard, A. J.; Zheng, X. L. Kinetic Study of Hydrogen Evolution Reaction over Strained MoS$_2$ with Sulfur Vacancies Using Scanning Electrochemical Microscopy. *J. Am. Chem. Soc.* **2016**, *138*, 5123−5129.

(25) Kim, W.; Javey, A.; Vermesh, O.; Wang, O.; Li, Y. M.; Dai, H. J. Hysteresis Caused by Water Molecules in Carbon Nanotube Field-Effect Transistors. *Nano Lett.* **2003**, *3*, 193−198.

(26) Hotoura, E.; Giapros, V.; Kostoula, A.; Spyrou, P.; Andronikou, S. Pre-Inflammatory Mediators and Lymphocyte Subpopulations in Preterm Neonates with Sepsis. *Inflammation* **2012**, *35*, 1094−1101.

(27) Faix, J. D. Biomarkers of Sepsis. *Crit. Rev. Clin. Lab. Sci.* **2013**, *50*, 23−36.

(28) Gullestad, L.; Ueland, T.; Vinge, L. E.; Finsen, A.; Yndestad, A.; Aukrust, P. Inflammatory Cytokines in Heart Failure: Mediators and Markers. *Cardiology* **2012**, *122*, 23−35.

(29) Schmitz, M. L.; Weber, A.; Roxlau, T.; Gaestel, M.; Kracht, M. Signal Integration, Crosstalk Mechanisms and Networks in The Function of Inflammatory Cytokines. *Biochim. Biophys. Acta, Mol. Cell Res.* **2011**, *1813*, 2165−2175.

(30) Mangan, D. F.; Welch, G. R.; Wahl, S. M. Lipopolysaccharide, Tumor-Necrosis-Factor-Alpha, and Il-1-Beta Prevent Programmed Cell-Death (Apoptosis) in Human Peripheral-Blood Monocytes. *J. Immunol.* **1991**, *146*, 1541−1546.

(31) Friedlander, R. M.; Gagliardini, V.; Rotello, R. J.; Yuan, J. Y. Functional Role of Interleukin 1 beta (IL-1 beta) in IL-1 Beta-Converting Enzyme-Mediated Apoptosis. *J. Exp. Med.* **1996**, *184*, 717−724.

(32) Dinarello, C. A. Historical Insights into Cytokines. *Eur. J. Immunol.* **2007**, *37*, S34−S45.

(33) Chiang, C. Y.; Hsieh, M. L.; Huang, K. W.; Chau, L. K.; Chang, C. M.; Lyu, S. R. Fiber-Optic Particle Plasmon Resonance Sensor for Detection of Interleukin-1 Beta in Synovial Fluids. *Biosens. Bioelectron.* **2010**, *26*, 1036−1042.

(34) Ebrahimi, B.; Tucker, S. L.; Li, D. H.; Abbruzzese, J. L.; Kurzrock, R. Cytokines in Pancreatic Carcinoma - Correlation with Phenotypic Characteristics and Prognosis. *Cancer* **2004**, *101*, 2727−2736.

(35) Mitsunaga, S.; Ikeda, M.; Shimizu, S.; Ohno, I.; Furuse, J.; Inagaki, M.; Higashi, S.; Kato, H.; Terao, K.; Ochiai, A. Serum Levels of IL-6 and IL-1 Beta Can Predict The Efficacy of Gemcitabine in Patients with Advanced Pancreatic Cancer. *Br. J. Cancer* **2013**, *108*, 2063−2069.

(36) Kern, J. A.; Lamb, R. J.; Reed, J. C.; Daniele, R. P.; Nowell, P. C. Dexamethasone Inhibition of Interleukin 1 Beta Production by Human Monocytes Posttranscriptional Mechanisms. *J. Clin. Invest.* **1988**, *81*, 237−244.

(37) Hideshima, S.; Sato, R.; Inoue, S.; Kuroiwa, S.; Osaka, T. Detection of Tumor Marker in Blood Serum Using Antibody-Modified Field Effect Transistor with Optimized BSA Blocking. *Sens. Actuators, B* **2012**, *161*, 146−150.

(38) Navazesh, M.; Christensen, C. M. A Comparison of Whole Mouth Resting and Stimulated Salivary Measurement Procedures. *J. Dent. Res.* **1982**, *61*, 1158−1162.

(39) Quereda, J.; Castellanos-Gomez, A.; Agrait, N.; Rubio-Bollinger, G. Single-Layer MoS$_2$ Roughness and Sliding Friction Quenching by Interaction with Atomically Flat Substrates. *Appl. Phys. Lett.* **2014**, *105*, 053111.

(40) Cai, B.; Wang, S.; Huang, L.; Ning, Y.; Zhang, Z.; Zhang, G. J. Ultrasensitive Label-Free Detection of PNA−DNA Hybridization by Reduced Graphene Oxide Field-Effect Transistor Biosensor. *ACS Nano* **2014**, *8*, 2632−2638.

(41) Gao, N.; Zhou, W.; Jiang, X.; Hong, G.; Fu, T. M.; Lieber, C. M. General Strategy for Biodetection in High Ionic Strength Solutions Using Transistor-Based Nanoelectronic Sensors. *Nano Lett.* **2015**, *15*, 2143−2148.